Supporting Information

for

A Germaaluminocene

Lena Albers*, Patrik Tholen, Marc Schmidtmann and Thomas Müller*

Institute of Chemistry, Carl von Ossietzky University Oldenburg, Carl von Ossietzky-Strasse 9-11,

D-26129 Oldenburg, Federal Republic of Germany, European Union

Table of Contents.

Experimental Part

General. All manipulations of air- and moisture-sensitive compounds were carried out under an argon 5.0 or nitrogen 5.0 atmosphere using Schlenk techniques or a standard glove box (Braun Unilab). Glassware was dried in an oven at T = 120 °C and evacuated prior to use. The solvents diethylether and ^{n}hexane were dried over sodium and distilled under a nitrogen atmosphere. Benzene-d_6 and toluene-d_8 were stored over molecular sieves (4 Å) after drying over potassium. Dipotassiumgermacyclopenta-dienediide $K_2[\mathbf{1}]$[1], (pentamethylcyclopentadienyl)borondichloride[2] and (pentamethylcyclopen-tadienyl)aluminiumdichloride[3] were prepared according to modified literature procedures.

NMR spectroscopy. NMR spectra were recorded on Bruker Fourier 300, Bruker Avance DRX 500, Bruker Avance III 500 spectrometers. ^{1}H NMR spectra were calibrated against the residual proton signal of the solvent as internal reference (benzene-d_6: $\delta^1H(C_6D_5H)$ = 7.16, toluene-d_8: $\delta^{13}C(C_7D_7H)$ = 2.08). ^{13}C NMR spectra were calibrated by using the central line of the solvent signal (benzene-d_6: $\delta^{13}C(C_6D_6)$ = 128.0, toluene-d_8: $\delta^{13}C(C_7D_8)$ = 20.4). ^{29}Si NMR and ^{11}B spectra were calibrated against external standards ($\delta^{29}Si(Me_2SiHCl)$ = 11.1 versus tetramethylsilane (TMS), $\delta^{11}B(BF_3\cdot Et_2O)$ = 0.0). The ^{29}Si{^{1}H} INEPT spectra were recorded with delays D3 = 0.0086 s and D4 = 0.313 s. For a clear assignment of the signals two-dimensional experiments, such as ^{1}H^{13}C HMQC and ^{1}H^{13}C HMBC spectra were recorded. The corresponding spectrometer frequencies and temperatures are indicated individually for every spectrum below.

Mass spectrometry. Mass Spectrum of germaaluminocene **3** was recorded with a Thermo Scientific DFS - High Resolution Magnetic Sector MS (HV-Emitter: 8kV, emitter heating current (EHC) Ramp: 21 mA/min, emitter heating current (EHC) max Ramp: 95mA). Mass Spectrum of germanium borole complex **2c** was not possible to obtain. Due to the reactivity against moisture and air mass peaks were not detectable by LIFDI-, EI-, ESI- nor APCI-experiments.

Combustion analysis: For compounds **2c** and **3**, no meaningful elemental analysis for the bulk material was obtained due to incomplete combustion and carbide formation and due to their reactivity against moisture and air. Instead all available NMR spectra of the bulk material are provided in the supporting material.

Single X-ray diffraction. Single crystal X -ray data were measured on a Bruker AXS Apex II diffractometer (Mo-Kα radiation, λ= 0.71073Å, Kappa 4 circle goniometer, Bruker Apex II detector). The crystal was kept from 90.0 K to 243.0 K during data collection. Absorption corrections based on symmetry-related measurements (multi-scan) were performed with the program SADABS.[4] The structures were solved with the program SHELXS and refined with SHELXL.[5] Pertinent data are summarized in Table S1. Crystallographic data for the structure of compound **3** has been deposited

with the Cambridge Crystallographic Data Centre as supplementary publication no. CCDC 1969078. Copies of data can be obtained free of charge at: http://www.ccdc.cam.ac.uk/products/csd/request/.

Synthesis of Cp*BCl$_2$[2]

$$Cp^*\text{—}SiMe_3 \ + \ BCl_3 \ \xrightarrow[\text{- Me}_3\text{SiCl}]{\substack{CH_2Cl_2 \\ \text{-40 °C to r.t.}}} \ Cp^*\text{—}BCl_2$$
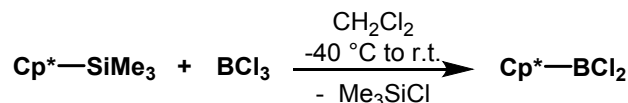
13.2 mL of a solution of BCl$_3$ in ^{n}hexane (c = 1 mol/L, 13.2 mmol) was added to 5 mL dichloromethane and was cooled to -40 °C. A solution of Cp*SiMe$_3$ (2.75 g, 13.2 mmol) in dichloromethane (5 mL) was added to the BCl$_3$-solution at -40 °C. The mixture was allowed to warm up to room temperature overnight. The dichloromethane was evaporated at 0 °C under reduced pressure. The product was then purifies by fractionate distillation (p = 0.5 mbar, T = 55 °C). Yield: 2.55 g (11.7 mmol, 89 %).

^{1}H NMR (499.9 MHz, 305.3 K, C$_6$D$_6$): δ = 1.62 (s, 15 H, Cp*-C$\underline{H}_3$).

^{13}C{^{1}H} NMR (125.7 MHz, 305.0 K, C$_6$D$_6$): δ = 12.4 (Cp*-$\underline{C}$H$_3$), 124.2 (Cp*$\underline{C}$).

^{11}B{^{1}H} NMR (160.4 MHz, 305.3 K, C$_6$D$_6$): δ = 60.2.
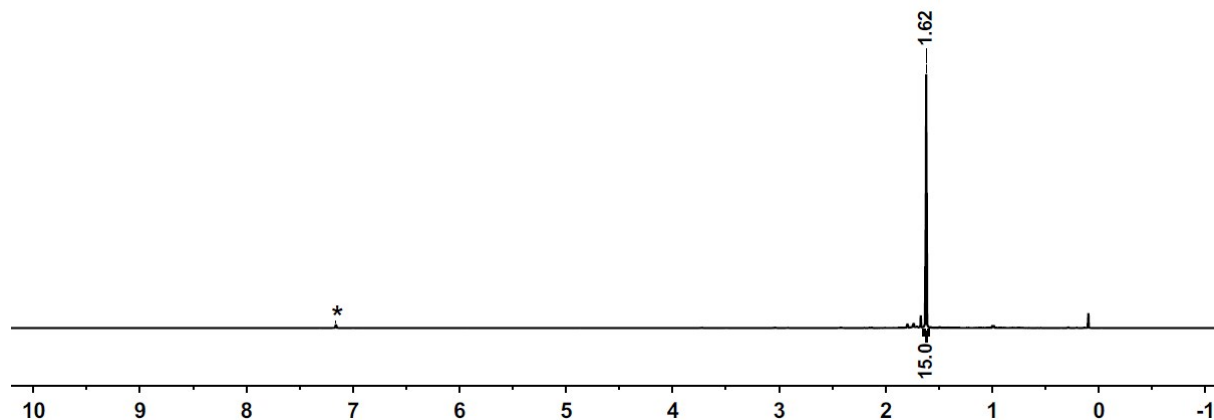
Figure S1. ^{1}H NMR spectrum (499.9 MHz, 305.3 K, C$_6$D$_6$) of Cp*BCl$_2$, *C$_6$D$_5$H.
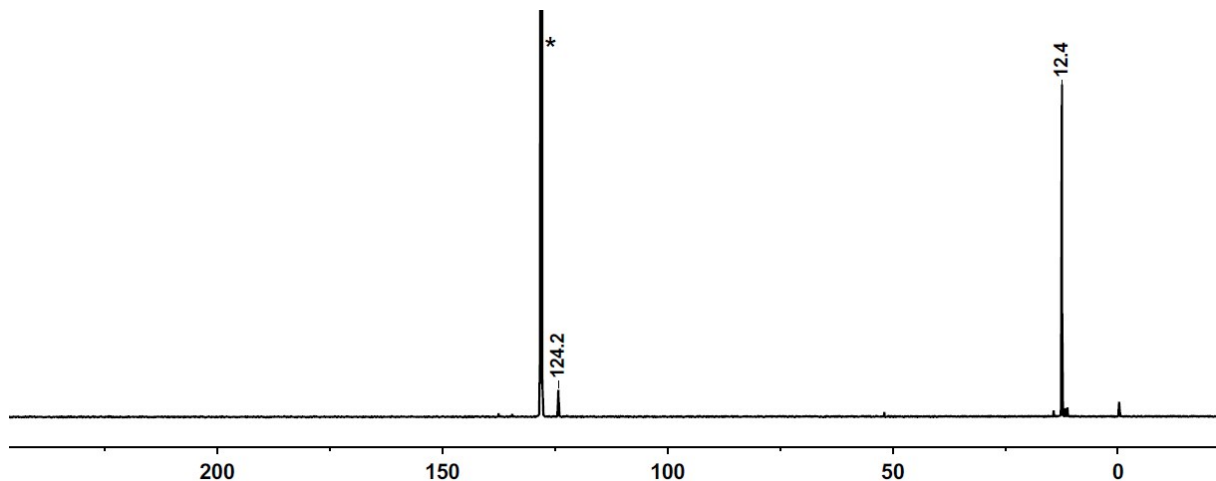
Figure S2. $^{13}C\{^1H\}$ NMR spectrum (125.7 MHz, 305.0 K, C_6D_6) of Cp*BCl$_2$, *C_6D_6.
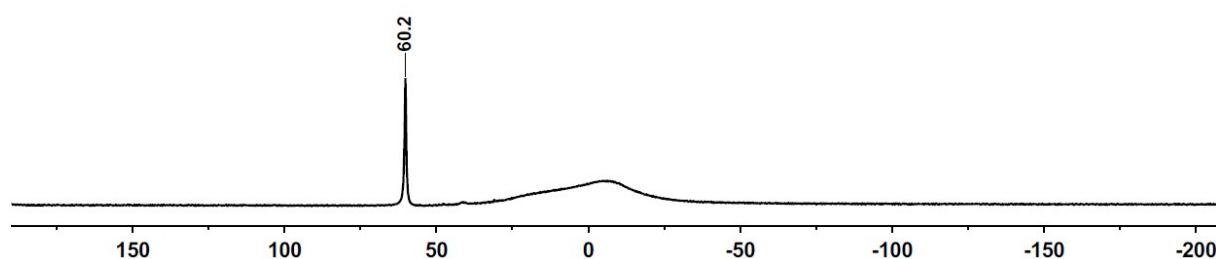
Figure S3. $^{11}B\{^1H\}$ NMR spectrum (160.4 MHz, 305.3 K, C_6D_6) of Cp*BCl$_2$,

Synthesis of Cp*AlCl$_2$[3]

$$Cp^*\!-\!SiMe_3 \ + \ AlCl_3 \xrightarrow[\text{-Me}_3\text{SiCl}]{\overset{^n\text{hexane}}{69°C}} Cp^*\!-\!AlCl_2$$
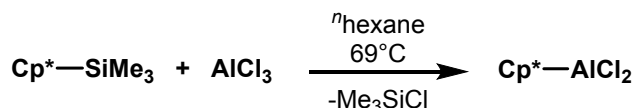
A solution of Cp*SiMe$_3$ (7.29 g, 35.0 mmol) in ^{n}hexane (5 mL) was added to a suspension of AlCl$_3$ (4.66 g, 35.0 mmol) in ^{n}hexane (5 mL) at room temperature. The mixture was refluxed for two hours. The hot solution was filtered through a frit and the filtrate was cooled to room temperature. The remaining solid on the frit was washed with ^{n}hexane. The yield was increased by refluxing the filtrate through the frit and thereby extracting the product. The solvent was removed in vacuum and the product was obtained as slightly purple solid. Yield: 4.66 g (20.0 mmol, 57 %).

^{1}H NMR (499.9 MHz, 305.1 K, C_6D_6): δ = 1.87 (s, 15 H, Cp*-C$\underline{H}_3$).

$^{13}C\{^1H\}$ NMR (125.7 MHz, 305.0 K, C_6D_6): δ = 10.7 (Cp*-$\underline{C}H_3$), 115.9 (Cp*$\underline{C}$).

$^{27}Al\{^1H\}$ NMR (130.3 MHz, 305.0 K, C_6D_6): δ = -49.8.
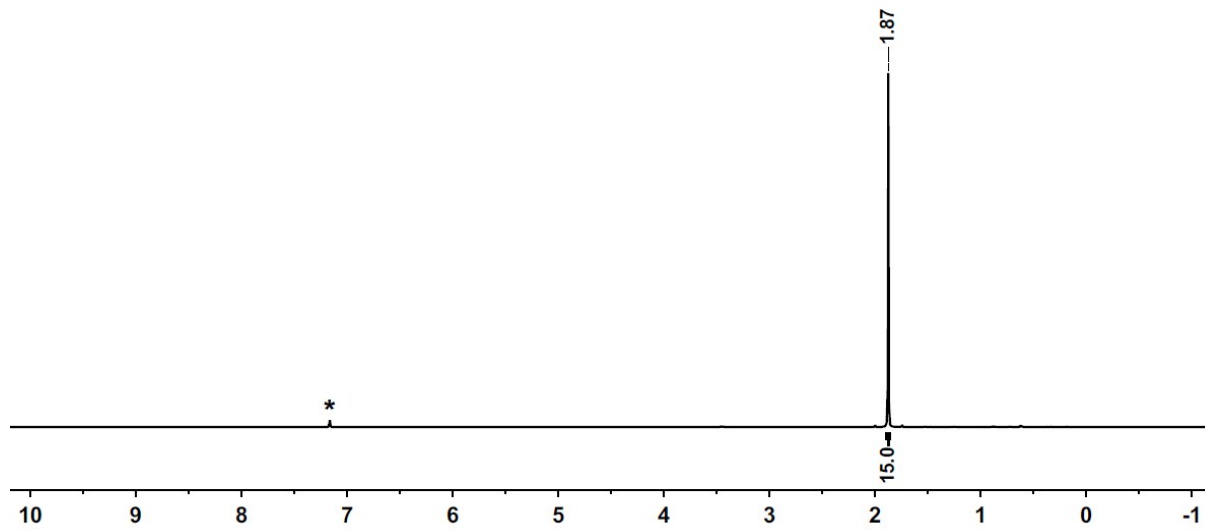
Figure S4. ^{1}H NMR spectrum (499.9 MHz, 305.1 K, C_6D_6) of Cp*AlCl$_2$, *C_6D_5H.
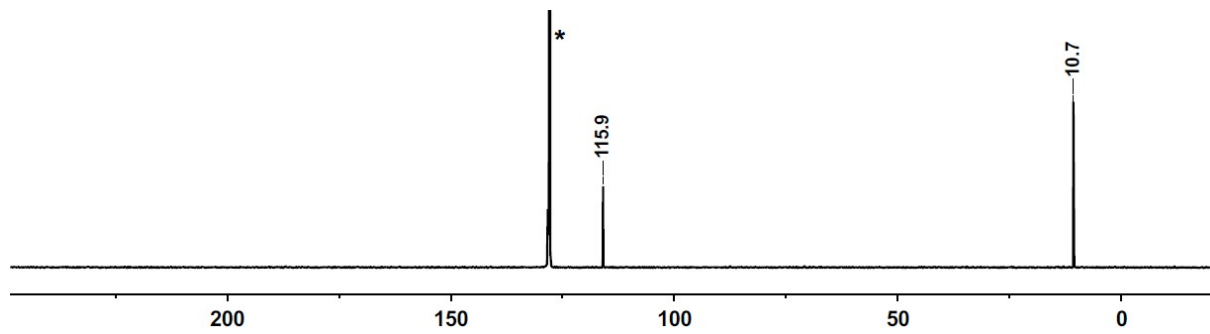
**Figure S5.** ^{13}C{^{1}H} NMR spectrum (125.7 MHz, 305.0 K, C_6D_6) of Cp*AlCl$_2$, *C_6D_6.
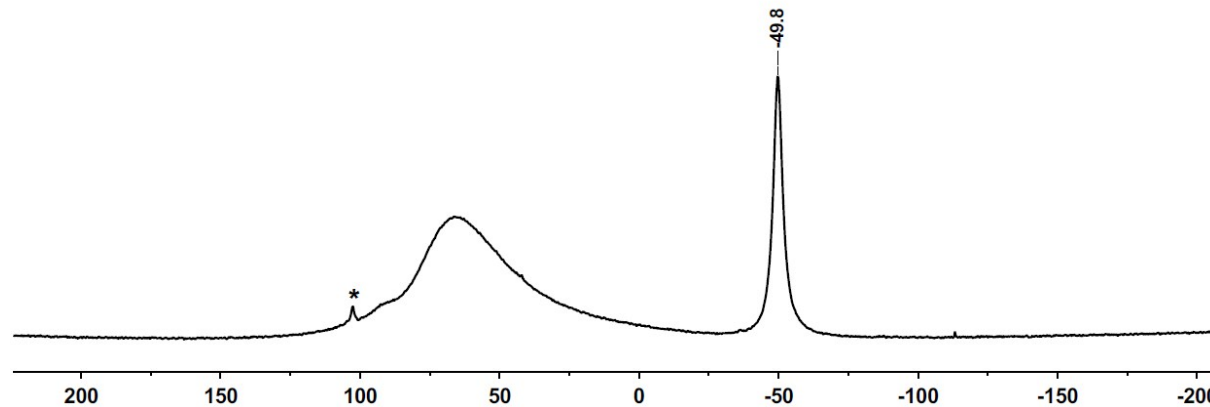
Figure S6. ^{27}Al{^{1}H} NMR spectrum (130.3 MHz, 305.0 K, C_6D_6) of Cp*AlCl$_2$, *AlCl$_4^-$ at δ^{27}Al = 103.

Cp*borole Ge(II) complex 2c:
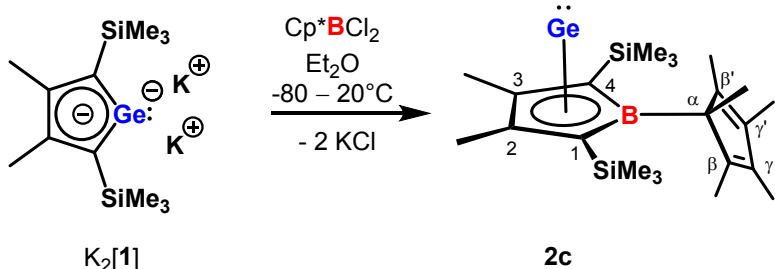
Dipotassiumgermacyclopentadienediide K$_2$[**1**] in Et$_2$O (0.5 mmol) was prepared in the glovebox and transferred to a Schlenk tube. A second Schlenk tube was filled with Et$_2$O (5 mL) and (penta-methylcyclopentadienyl)borondichloride (0.5 mmol, 109 mg). Both solutions were cooled to -80 °C and the borane solution was transferred to the dipotassiumgermacyclopentadienediide solution via a *Teflon* tube. The reaction mixture was stirred for one hour at -80 °C and was allowed to warm to room temperature over 19 hours. The precipitate was filtered off and the remaining solvent was removed from the filtrate under reduced pressure. The oily brown residue was dissolved in ^{n}hexane and filtered through silica gel. After evaporation of the solvent, the residue was dissolved in benzene-d$_6$ and analyzed by NMR spectroscopy. Yield: 78 mg (0.18 mmol, 35 %).

^{1}H NMR (499.9 MHz, 305.1 K, C$_6$D$_6$): δ = 0.07 (s, 9 H, Si(C$\underline{H}_3$)$_3$), 0.37 (s, 9 H, Si(C$\underline{H}_3$)$_3$), 1.48 (s, 3 H, C$^\alpha$-C$\underline{H}_3$), 1.82 (s, 3 H, C $^{\beta/\beta'}$-C$\underline{H}_3$), 1.85 (s, 3 H, (C$^{\gamma/\gamma'}$-C$\underline{H}_3$), 1.89 (s, 3 H, C$^{\gamma/\gamma'}$-C$\underline{H}_3$), 2.02 (s, 3 H, C$^{2/3}$-C$\underline{H}_3$), 2.03 (s, 3 H, C$^{2/3}$-C$\underline{H}_3$), 2.06 (s, 3 H, C $^{\beta/\beta'}$-C$\underline{H}_3$).

^{13}C{^{1}H} NMR (125.8 MHz, 305.0 K, C$_6$D$_6$): δ = 2.8 (Si(CH$_3$)$_3$), 5.1 (Si(CH$_3$)$_3$), 11.6 (CH$_3$), 12.0 (CH$_3$), 13.0 (CH$_3$), 13.9 (CH$_3$), 15.2 (CH$_3$), 15.5 (CH$_3$), 26.5 (C$^\alpha$-CH$_3$), 53.6 (C$^\alpha$), 99.3 (C$^{1/4}$), 99.8 (C$^{1/4}$), 131.6 (C$^{\gamma/\gamma'}$), 133.6 (C$^{2/3}$), 133.8 (C$^{\gamma/\gamma'}$), 134.8 (C$^{2/3}$), 144.2 (C$^{\beta/\beta'}$), 148.3 (C $^{\beta/\beta'}$).

^{11}B{^{1}H} NMR (160.5 MHz, 305.1 K, C$_6$D$_6$): δ = 37.2.

^{29}Si{^{1}H} INEPT NMR (99.4 MHz, 305.1 K, C$_6$D$_6$): δ = -9.1 (SiMe$_3$), -8.7 (SiMe$_3$).
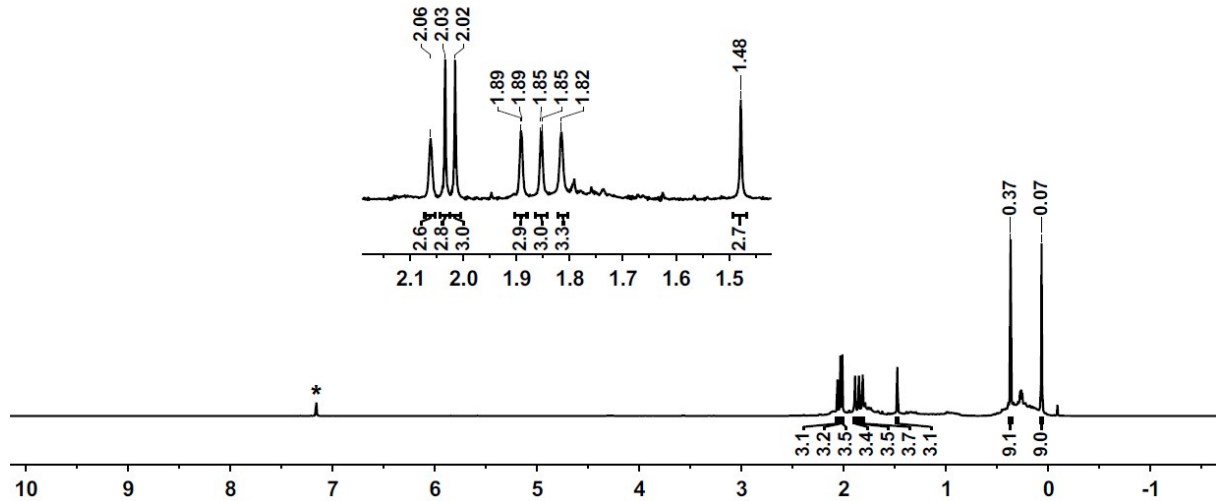
Figure S7. ^{1}H NMR spectrum (499.9 MHz, 305.1 K, C_6D_6) of the germanium borole complex **2c**, * C_6D_5H.
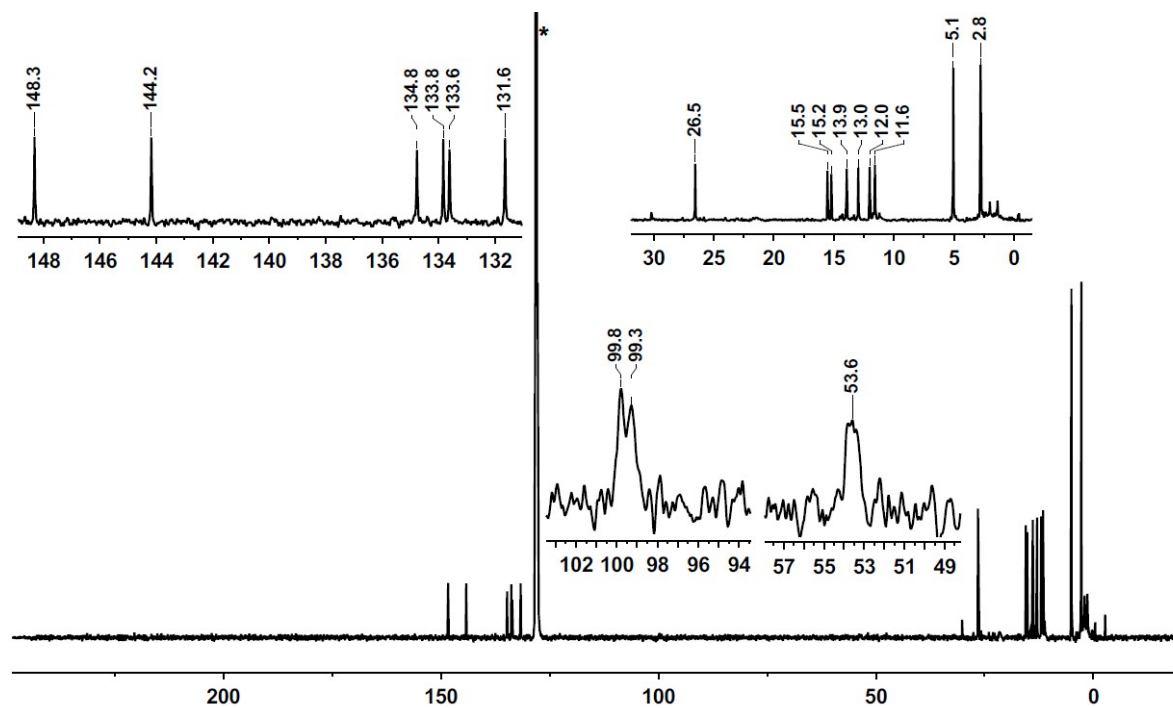
Figure S8. $^{13}C\{^1H\}$ NMR spectrum (125.7 MHz, 305.0 K, C_6D_6) of the germanium borole complex **2c**,
* C_6D_6
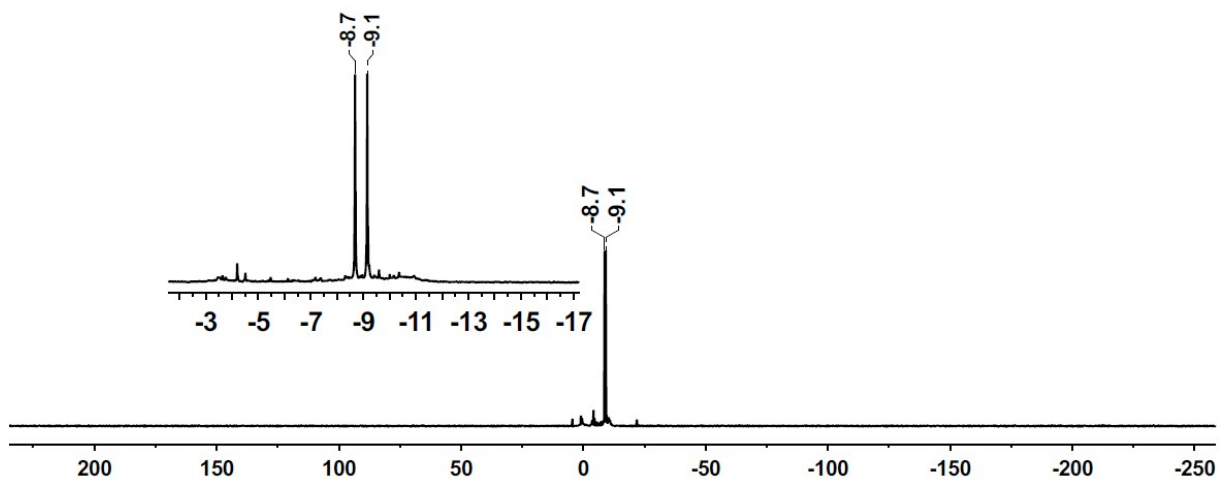
Figure S9. ^{29}Si{^{1}H} INEPT NMR spectrum (99.3 MHz, 305.0 K, C$_6$D$_6$,) of the germanium borole complex **2c**.
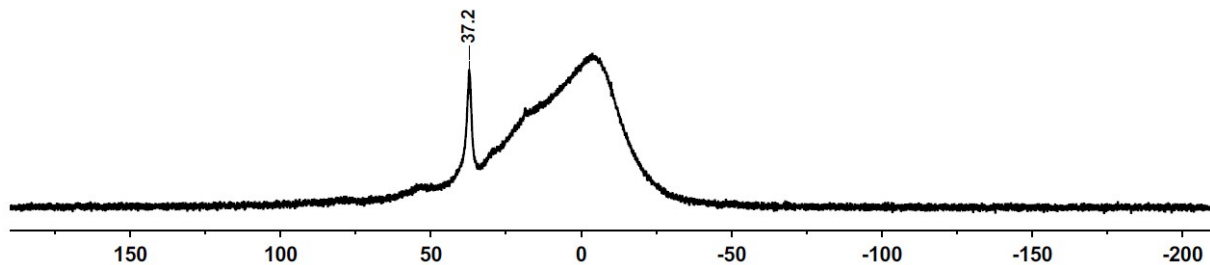
Figure S10. ^{11}B{^{1}H} NMR spectrum (160.4 MHz, 305.1 K, C$_6$D$_6$) of the germanium borole complex **2c**.
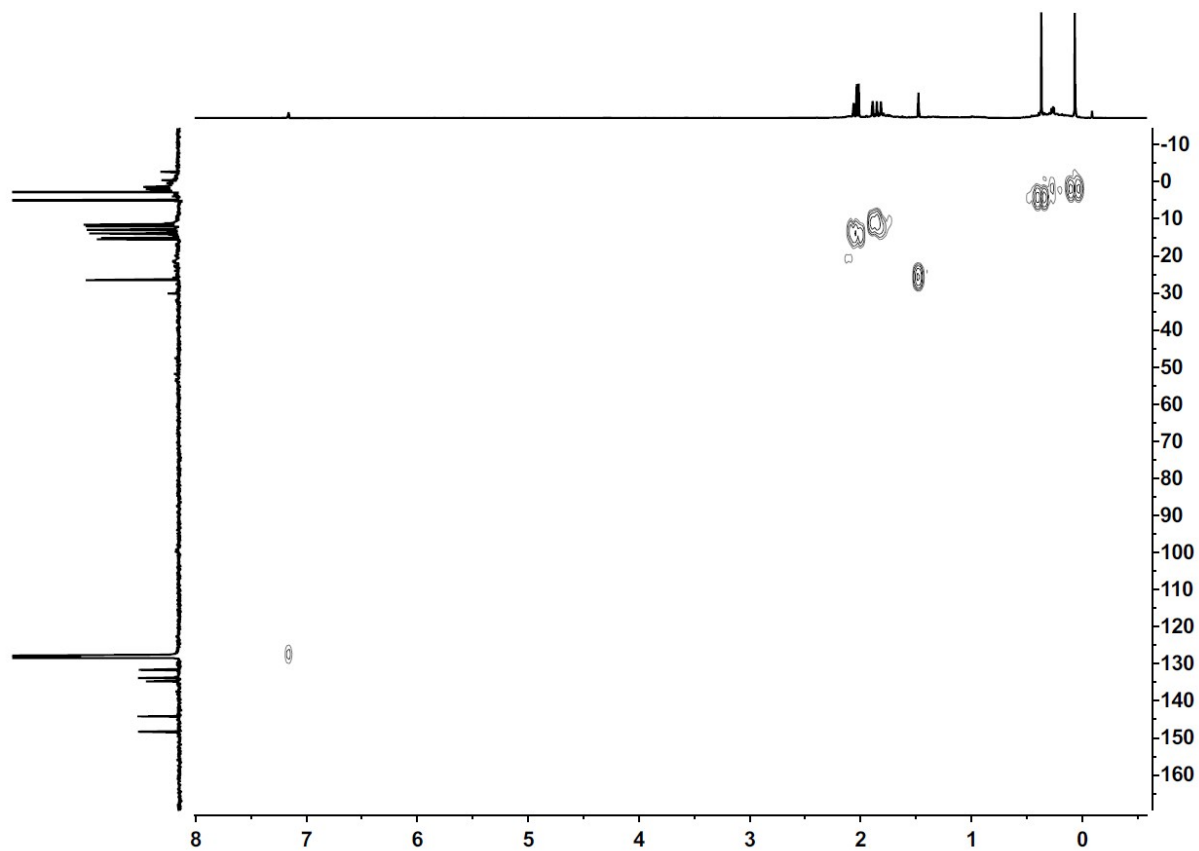
Figure S11. $^{1}H^{13}C$ HMQC NMR spectrum (499.9 MHz/125.7 MHz, 305.0 K, C_6D_6) of the germanium borole complex **2c**.
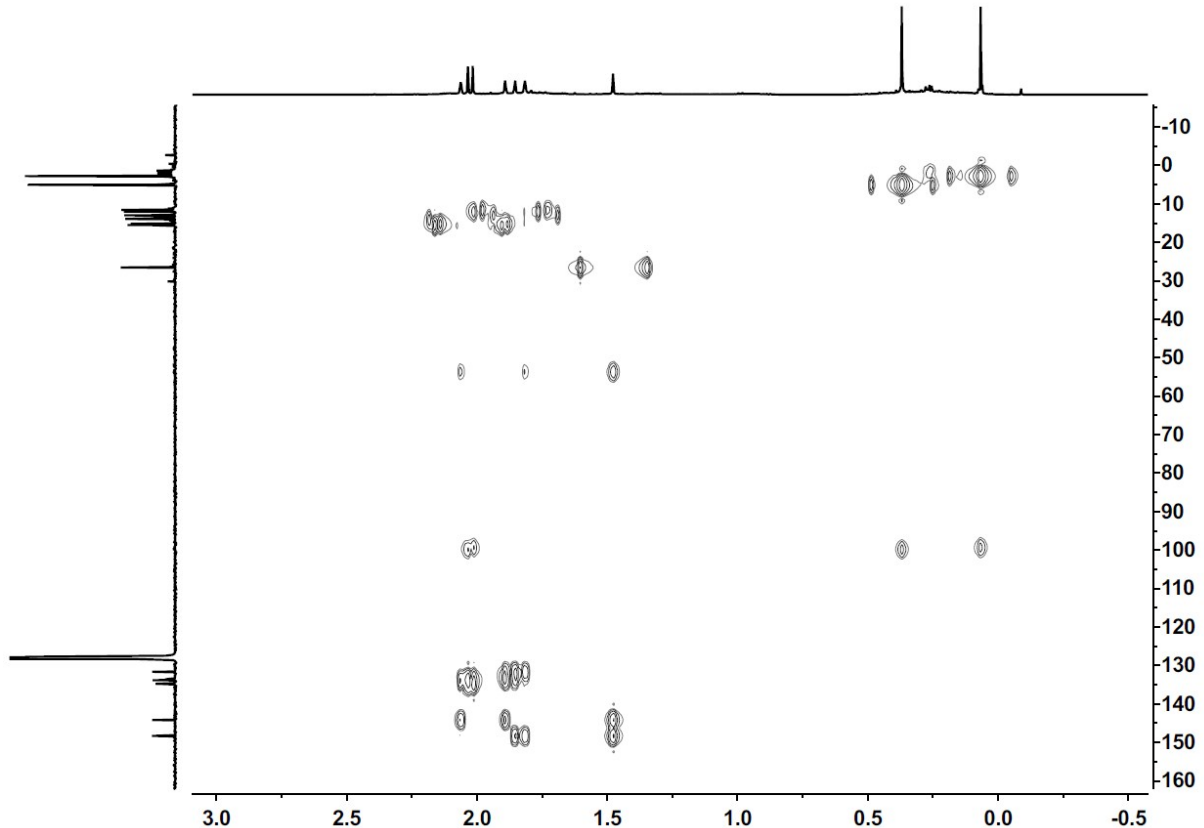

Figure S12. $^{1}H^{13}C$ HMBC NMR spectrum (499.9 MHz/125.7 MHz, 305.0 K, C_6D_6) of the germanium borole complex **2c**.

Germaaluminocene 3:
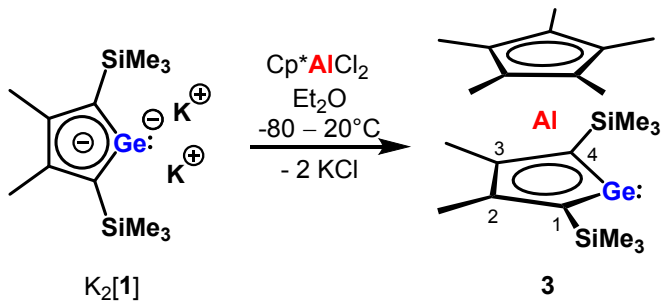
Dipotassiumgermacyclopentadienediide $K_2[1]$[1] in Et_2O (0.5 mmol) was prepared in the glovebox and transferred to a Schlenk tube. A second Schlenk tube was filled with Et_2O (5 mL) and (penta-methylcyclopentadienyl)aluminumdichloride (0.5 mmol, 117 mg). Both solutions were cooled to -80 °C and the alane solution was transferred to the dipotassiumgermacyclopentadienediide solution via a *Teflon* tube. The reaction mixture was stirred for one hour at -80 °C, the cold bath was removed and the mixture stirred at room temperature for two hours. The solvent was removed in vacuum, the residue was dissolved in ^{n}hexane. After filtration the solvent of the filtrate was removed in vacuum. The residue was dissolved in toluene-d_8 and analyzed by NMR spectroscopy. Single crystals suitable for XRD analysis were obtained from ^{n}hexane at 8 °C within one day. Yield: 65 mg (0.14 mmol, 28 %)

^{1}H NMR (500.1 MHz, 305.0 K, C_7D_8): δ = 0.45 (s, 18 H, $C^{1/4}Si(C\underline{H}_3)_3$), 1.69 (s, 15 H, Cp*-C$\underline{H}_3$), 2.34 (s, 6 H, $C^{2/3}C\underline{H}_3$).

^{13}C{^{1}H} NMR (125.8 MHz, 305.0 K, C_7D_8): δ = 3.9 (Si($\underline{C}H_3)_3$), 10.8 (Cp*-CH_3), 20.9 ($C^{2/3}\underline{C}H_3$), 114.9 (Cp*$\underline{C}$), 149.9 ($\underline{C}^{2/3}$), 167.0 ($\underline{C}^{1/4}$).

^{29}Si{^{1}H} INEPT NMR (99.4 MHz, 305.0 K, C_7D_8): δ = -9.5 ($\underline{Si}(CH_3)_3$).

^{27}Al{^{1}H} NMR (130.3 MHz, 305.0 K, C_7D_8): δ = -77.4.

MS (70 eV, LIFDI): m/z = calc.: 460.2   ($M^+(^{12}C_{22}{}^1H_{39}{}^{27}Al^{74}Ge^{28}Si_2)$)
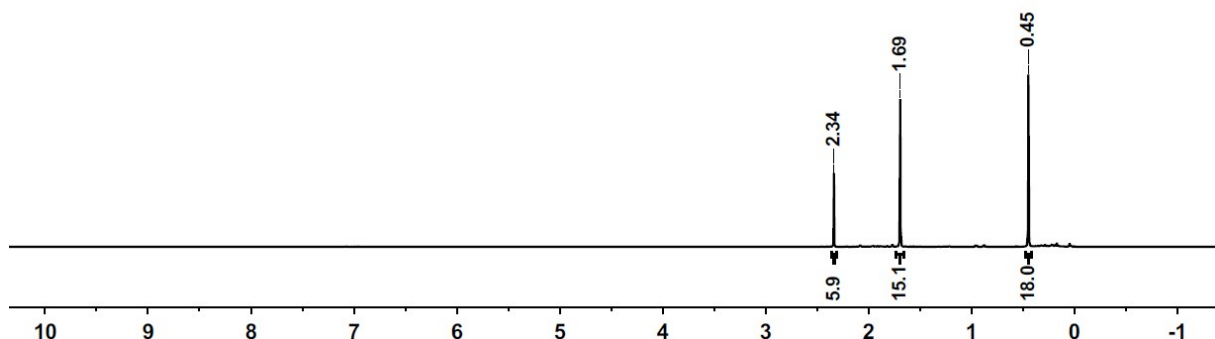
Figure S13. ^{1}H NMR spectrum (499.9 MHz, 305.0 K, C_7D_8) of germaaluminocene **3**.
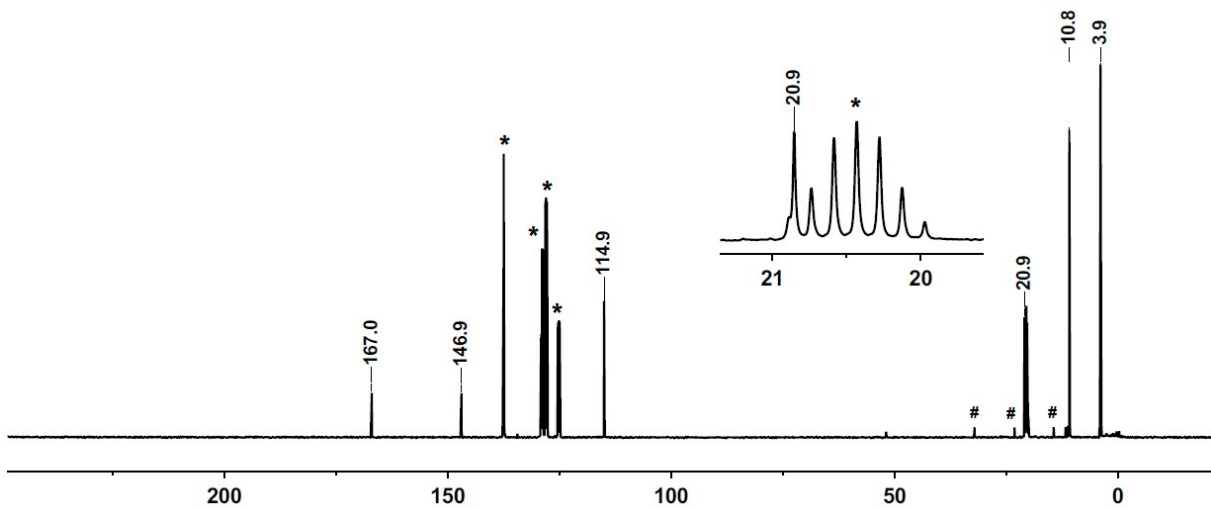
Figure S14. $^{13}C\{^1H\}$ NMR spectrum (125.8 MHz, 298.2 K, C_7D_8) of germaaluminocene **3**, * C_7D_8, # ^{n}hexane.
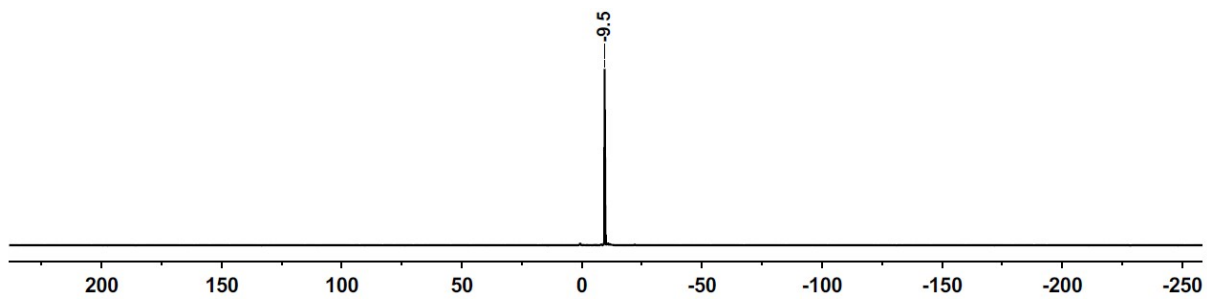
Figure S15. $^{29}Si\{^1H\}$ INEPT NMR spectrum (99.3 MHz, 305.0 K, C_7D_8) of germaaluminocene **3**.
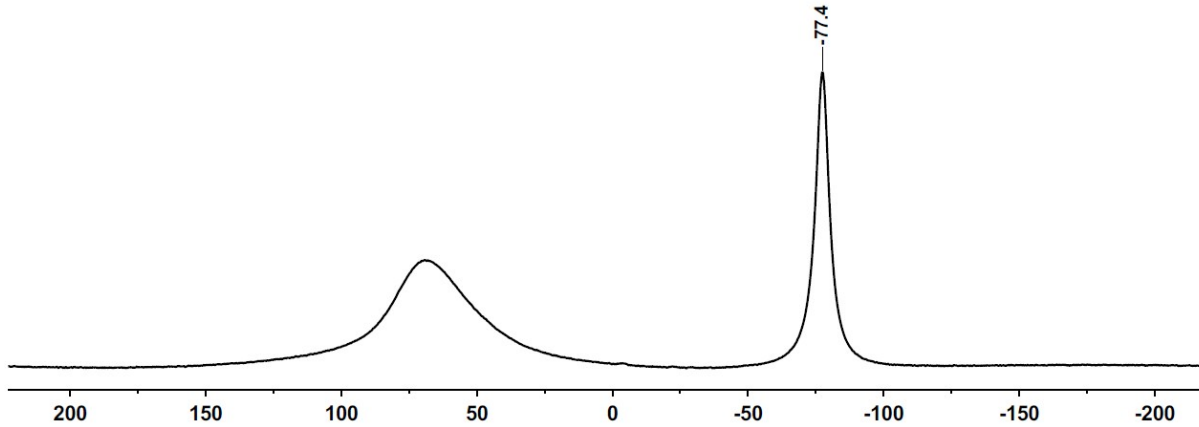
Figure S16. $^{27}Al\{^1H\}$ NMR spectrum spectrum (130.3 MHz, 305.0 K, C_7D_8 of germaaluminocene **3**.
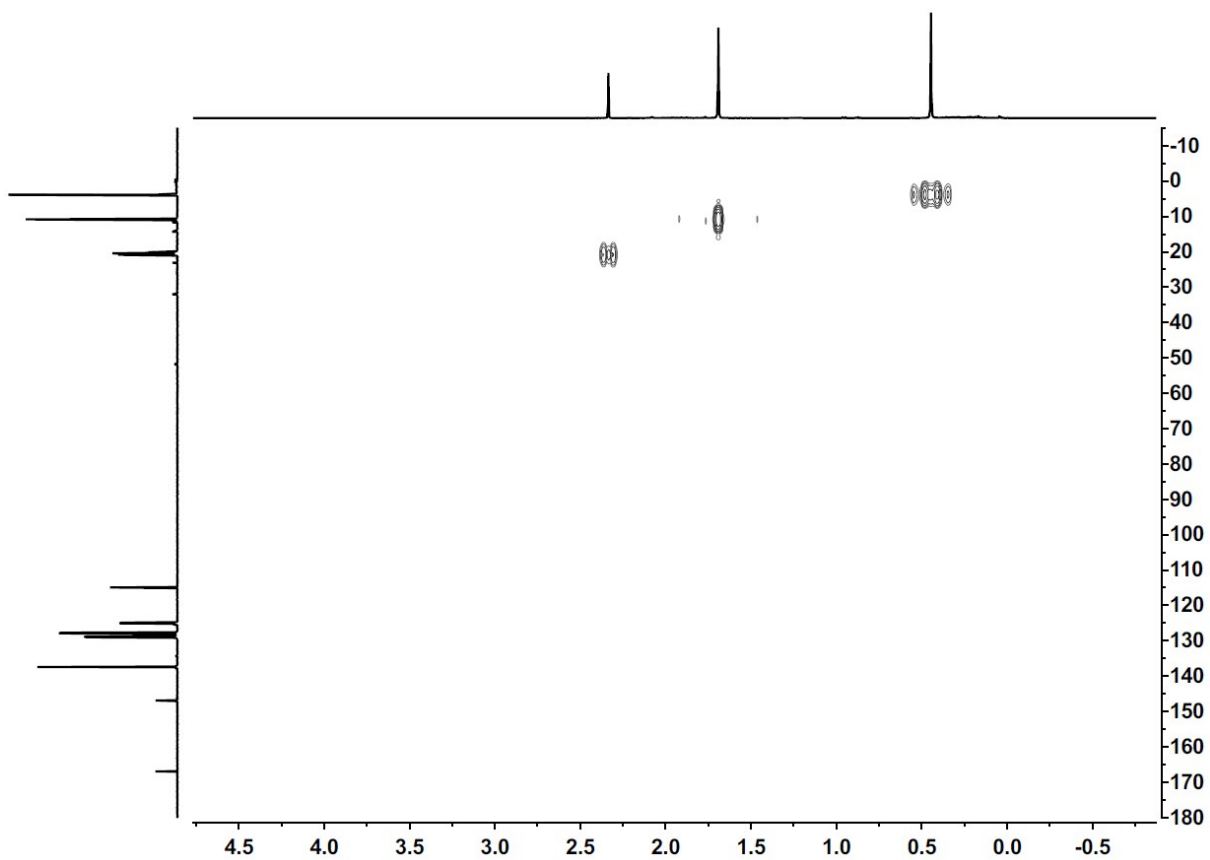
Figure S17. $^1H^{13}C$ HMQC NMR spectrum (500.1 MHz/125.8 MHz, 299.0 K, C_7D_8) of germaaluminocene **3**.
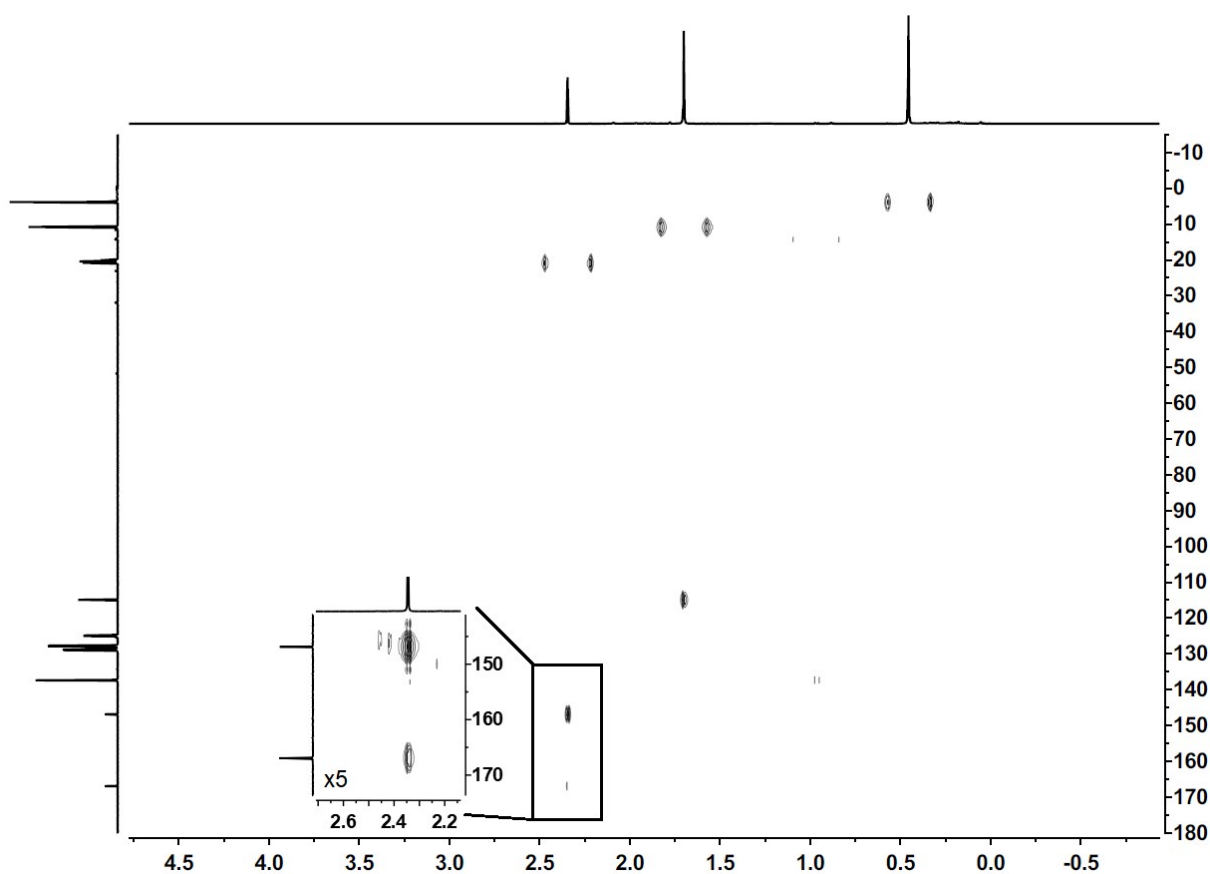
Figure S18. $^1H^{13}C$ HMBC NMR spectrum (500.1 MHz/125.8 MHz, 298.9 K, C_7D_8) of germaaluminocene **3**.

Low-temperature NMR experiments of germaaluminocene 3 at -90 °C
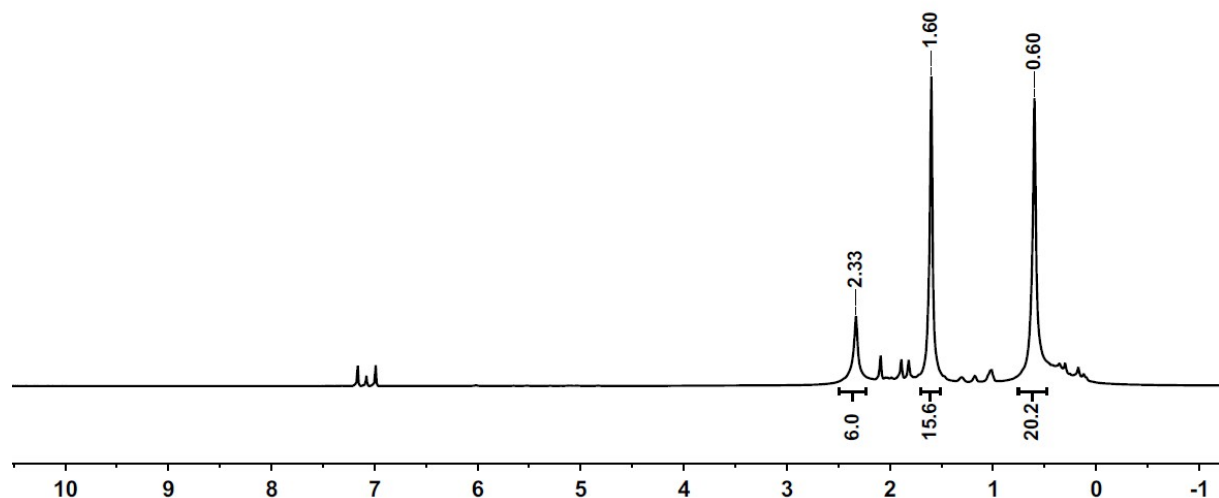
Figure S19. ^{1}H NMR spectrum (499.9 MHz, 182.8 K, C$_7$D$_8$) of germaaluminocene **3**.
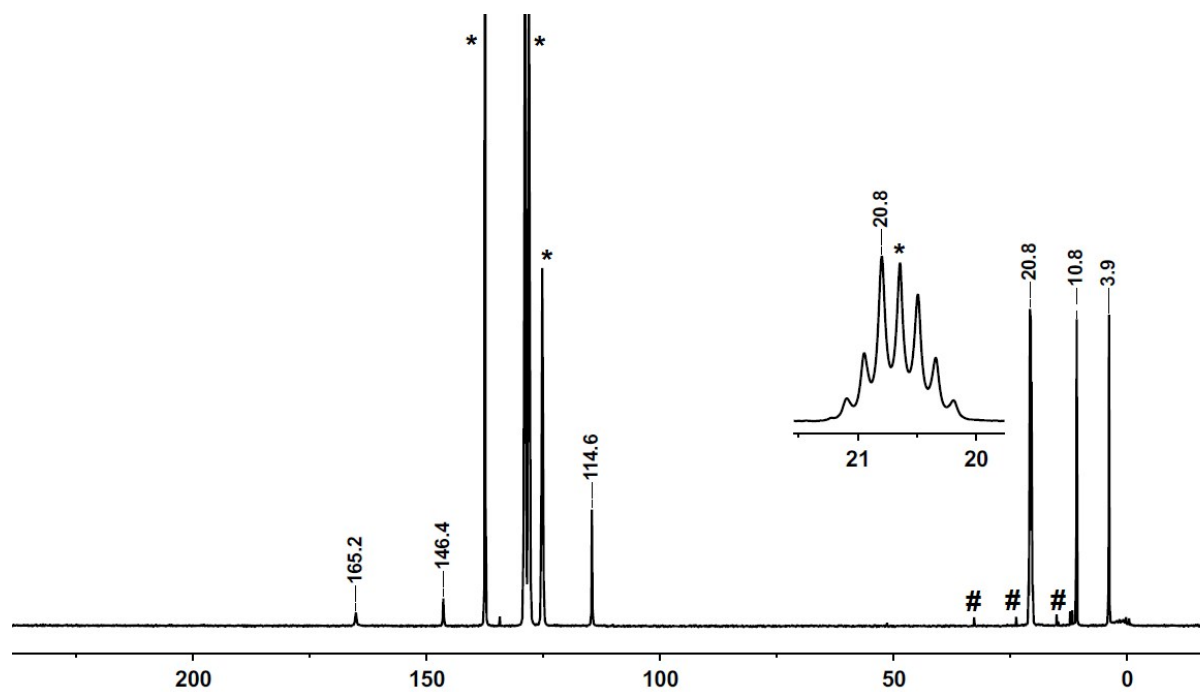
Figure S20. ^{13}C{^{1}H} NMR spectrum (125.7 MHz, 182.8 K, C$_7$D$_8$) of germaaluminocenene **3**, * C$_7$D$_8$, # ^{n}hexane.

Molecular structure of germaaluminocene 3 from single crystal X-ray diffraction analysis.
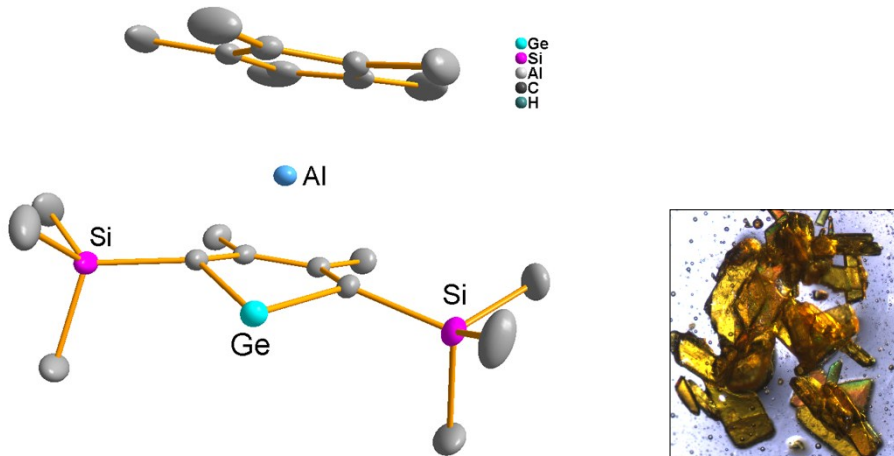
Table S1. Summary of crystallographic data of germaaluminocene **3**.

Empirical formula	$C_{22}H_{39}AlGeSi_2$	
Formula weight	459.28	
Temperature	120(2) K	
Wavelength	0.71073 Å	
Crystal system	Monoclinic	
Space group	$P2_1/n$	
Unit cell dimensions	a = 9.6414(5) Å	a = 90°.
	b = 13.3432(7) Å	b = 95.4683(19)°.
	c = 19.6279(10) Å	g = 90°.
Volume	2513.6(2) Å^3	
Z	4	
Density (calculated)	1.214 Mg/m^3	
Absorption coefficient	1.344 mm^{-1}	
F(000)	976	
Crystal size	0.150 x 0.130 x 0.070 mm^3	
θ range for data collection	1.848 to 34.968°	
Index ranges	-15<=h<=15, -21<=k<=21, -31<=l<=31	
Reflections collected	247473	
Independent reflections	11052 (R_{int} = 0.0399)	
Observed reflections (I > 2(I))	9829	
Completeness to θ = 34.968°	100.00%	
Absorption correction	Semi-empirical from equivalents	
Max. and min. transmission	1.0000 and 0.8790	
Refinement method	Full-matrix least-squares on F^2	
Data / restraints / parameters	11052 / 0 / 343	
Goodness-of-fit on F^2	1.092	
Final R indices (I > 2σ(I))	R_1 = 0.0284, wR_2 = 0.0792	
R indices (all data)	R_1 = 0.0336, wR_2 = 0.0825	
Extinction coefficient	n/a	
Largest diff. peak and hole	1.556 and -0.406 e/Å^3	

Table S2. Experimental and calculated (italic, at M06-2X/6-311+G(d,p)) structural data of compounds relevant for the discussion.

	3	3M	K$_2$[1][1]	8[AlCl$_4$][6]	9[7]	11[8]
Ge–Al	248.8 (*250.3*)	*250.5*				
Al–C1	212.9 (*213.5*)	*212.7*				
Al–C4	214.2 (*213.7*)	*212.7*				
Al–C2	228.2 (*228.7*)	*226.1*				
Al–C3	227.6 (*226.6*)	*226.1*				
Ge–C1	199.9 (*200.6*)	*200.0*	194.9 (*198.2*)			
Ge–C4	200.0 (*200.6*)	*200.0*	194.2 (*198.2*)			
C1–C2	144.7 (*144.4*)	*142.6*	141.5 (*142.6*)			
C3–C4	144.6 (*144.4*)	*142.6*	142.0 (*142.6*)			
C2–C3	142.1 (*141.8*)	*141.1*	139.5 (*142.2*)			
Al–Ctr	186.6			176.9	180.2	206.3
Al–C(Cp*)	217–228 *215–230*	216–234		213–218	217.0	238.8

Table S3. Selected experimental and calculated ^{13}C, ^{11}B and ^{27}Al NMR chemical shifts.

		$\delta^{13}C^{exp}$	$\delta^{13}C^{calc\,e)}$	$\delta^{11}B^{exp}$ ($\delta^{11}B^{cal})^{e)}$	$\delta^{27}Al^{exp}$ ($\delta^{27}Al^{calc})^{e)}$
2a[a) 9]	C2/C3	127.7	122.0	31 (29)	
	C1/C4	103.2	94.7		
2b[a) 9]	C2/C3	129.3	124.0	29 (24)	
	C1/C4	105.5	101.1		
2c[a)]	C2/C3 C1/C4	133.3, 133.8 99.8, 99.3	126.6, 127.3 88.7, 92.6	37 (30)	
	Cα-Cγ	53.6 131.6,134.8 144.2, 148.3	53.4 128.7, 130.2 140.8, 142.5		
K$_2$[**1**][b) 1]	C2/C3	130.8			
	C1/C4	156.2			
3[c)]	C2/C3 C1/C4 C(Cp*)	147.9 167.0 114.9, 10.8	137.7 156.6 108.9, 16.3		-77 (-71)
4[a) 10]	C2/C3	128.4		25	-86
	C1/C4	118.0			
Li$_2$[**6**][a) 11]	C2/C3	112.6	97.4		198 (193)
	C1/C4	102.6	76.6		
8^{+}[d) 12]	C(Cp*)	118.8, 10.5			-115 (-96) ((Cp*)$_2$Al$^+$)
9[a) 7]	C(Cp*)			-33 (-30)	-59 (-50)
10[a) 13]	C(Cp*)	115.9, 8.4			-116 (Cp*Al)
11[c) 14]	C(Cp*)				-150 (-137)
[**11**]$_4$[c) 14]	C(Cp*)	114.2, 11.4			-81
7[c) 15]					64

a) C$_6$D$_6$, r.t. b) THF-d$_8$, r.t. c) C$_7$D$_8$, r.t. d) CDCl$_3$, r.t.

e) calculated at M06-L/6-311G(2d,p)//M06-2X/6-311+G(d,p)

Computational Details.

All quantum chemical calculations were carried out using the Gaussian16 package.[16] The NBO analyses[17] were performed with the version 6.0 which was implemented in the G09 D.01[18] version of the Gaussian program.[19] The AIMALL program was used to perform the QTAIM analysis.[20] For the visualization of the natural bond orbitals the program Jmol was used.[21]

The molecular structure optimizations were performed using the M06-2X[22] functional along with the 6-311+G(d,p) basis set. The level of theory is justified by the close agreement between calculated and experimentally determined structural parameter (see Table S2), the largest difference in atomic distances between calculated data for **3** and for the close model **3M** on one hand and experimental values for **3** on the other hand is less than 2%) and by the close agreement between calculated NMR chemical shifts based on the DFT-optimized molecular structure of **3**.

Every stationary point was identified by a subsequent frequency calculation either as minimum (Number of imaginary frequencies NIMAG: 0) or transition state (NIMAG: 1) .The SCF energies, E(SCF), for all optimized molecular structures obtained with these methods are given in Table S4, Table S6 and Table S7. The absolute, G^{298}, and relative, $G^{298,rel}$, computed Gibbs free energies at T = 298.15 K and p = 0.101 MPa (1 atm) in the gas phase, are also given in Table S4, Table S6 and Table S7. Intrinsic reaction coordinate (IRC) calculations were used to connect transition state structures with the appropriate molecular structures of intermediates.[23] All corresponding computed molecular structures are given in the xyz-files. NMR chemical shift computations were performed using the GIAO method as implemented in Gaussian 16 and the M06-L functional[22] along with the 6-311G(2d,p) basis set for molecular structures obtained at the M06-2X/6-311+G(d,p) of theory. For the NBO and QTAIM analysis a density obtained using the M06-2X functional along with the 6-311+G(d,p) basis set was applied.

Table S4. Absolute (E) and free Gibbs enthalpies (G^{298}) for compounds **2c**, $K_2[\mathbf{1}]$ **14**, **3**, **3M**, **8$^+$**, **9**, **11**, $Li_2[\mathbf{6}]$, Ph_4Al^-, $Ph_3Al(Et_2O)$, $(Cp^*AlCl_2)_2$ and H_4Al^- at the M06-2X/6-311+G(d,p) level of theory, partially used for Table S3 and Figure 6.

Compound	E [a.u.]	NIMAG, $\tilde{\nu}$ [cm^{-1}] ZPVE [kJ mol^{-1}]	G^{298} [a.u.]
2c	-3542.52813	0; -; 1463	-3542.03505
11	-632.45630	0; -; 585	-632.27401
8$^+$	-1022.31179	0; -; 1176	-1021.91902
9	-2840.71992	0; -; 1002	-2840.41694
3	-3760.11906	0; -; 1447	-3759.63259
3M	-2667.68380	0; -; 397	-2667.57074
14	-3760.12000	0; -; 1447	-3759.62407
$K_2[\mathbf{1}]$	-4327.54568	0; -; 850	-4327.28117
$Li_2[\mathbf{6}]$	-1429.98114	0; -; 1908	-1429.32189
Ph_4Al^-	-1168.94167	0; -; 948	-1168.63888
$Ph_3Al(Et_2O)$	-1170.90582	0; -; 1085	-1170.54961
$(Cp^*AlCl_2)_2$	-3106.05887	0; -; 1195	-3105.67129
H_4Al^-	-244.81134	0; -; 64	-244.80652

Table S5. Experimental and calculated ^{27}Al NMR chemical shifts of selected compounds calculated at the M06-L/6-311G(2d,p) level of theory.

Compound	$\delta\,^{27}Al$ calc.[b]	$\delta^{27}Al$ exp.[a]	reference
11	-137	-150	[14, 24]
8$^+$	-96	-115	[12b]
9	-50	-59	[7]
3	-70	-77	this work
14	+21	-	this work
$Li_2[\mathbf{6}]$	+196	+198	[11]
Ph_4Al^-	+151	+133	[25]
$Ph_3Al(Et_2O)$	+162	+147	[25]
$(Cp^*AlCl_2)_2$	-39	-50	this work
Cp^*AlCl_2	-1	-	this work
H_4Al^-	+101	+101	Exp.[26]; calc.[14]

a) $\delta^{27}Al$ vs. $\delta^{27}Al([Al(H_2O)_6]^{3+}) = 0$; b) $\delta^{27}Al$ vs. $\delta^{27}Al(H_4Al^-) = +101$[14]
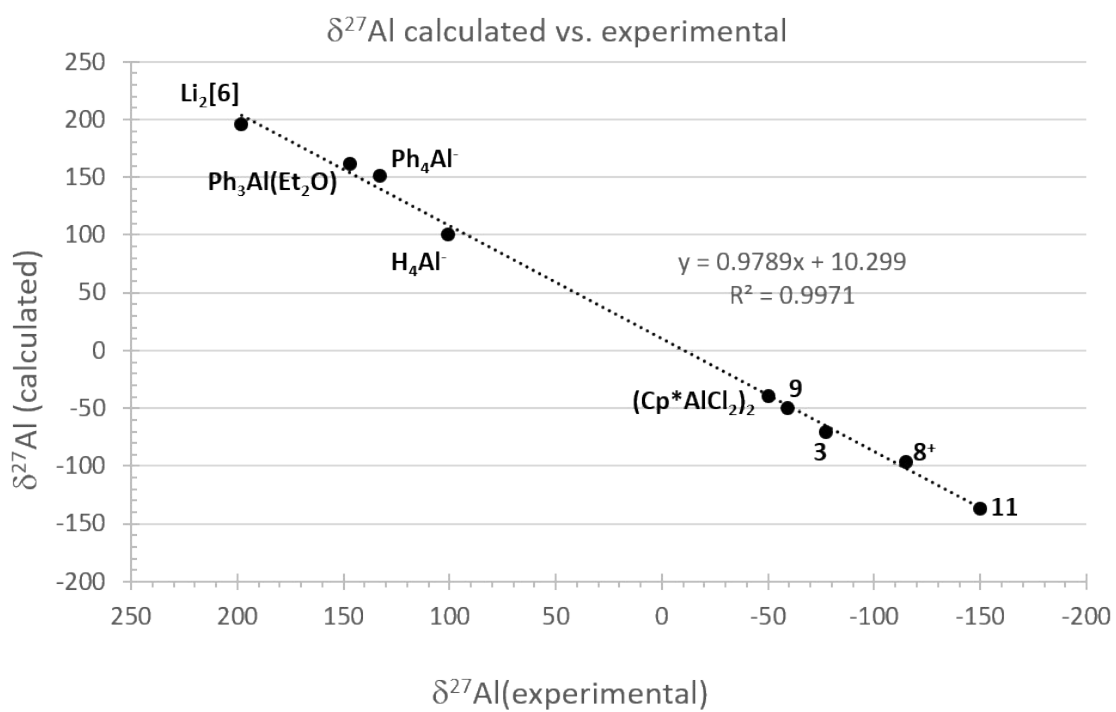
Figure S21. Plot of the calculated vs experimental ^{27}Al NMR chemical shifts (experimental δ^{27}Al vs. δ^{27}Al($[Al(H_2O)_6]^{3+}$) = 0 calculated at the M06-L/6-311G(2d,p) level of theory, δ^{27}Al vs. δ^{27}Al(H_4Al^-) = +101[14]).

Table S6. Absolute and relative energies (E and E^{rel}) and free Gibbs enthalpies (G^{298} and $G^{298\ rel}$) for compounds **3** $K_2[\mathbf{1}]$, **8**, Me_3Al^+ and MeAl(I) at the M06-2X/6-311+G(d,p) level of theory used for Figure 6.

Compound	E [a.u.]	NIMAG, $\tilde{\nu}$ [cm^{-1}] ZPVE [kJ mol^{-1}]	G^{298} [a.u.]
3	-3760.11906	0; -; 1447	-3759.63259
$K_2[\mathbf{1}]$	-4327.54568	0; -; 850	-4327.28117
8$^+$	-1022.31179	0; -; 1176	-1021.91902
Me_3Al	-362.13271	0; -; 279	-362.06101
MeAl(I)	-282.280130	0; -; 88	-282.26927

Table S7. Absolute and relative energies (E and E^{rel}) and free Gibbs enthalpies (G^{298} and $G^{298,rel}$) of compounds **2c**, **3**, **12**, **13**, **17** and related model compounds and transition states connecting them at the M06-2X/6-311+G(d,p) level of theory. The corresponding free enthalpy diagram is shown in Figure S23.

Compound	E [a.u.]	E^{rel} [kJ mol^{-1}]	NIMAG; $\tilde{\nu}$ [cm^{-1}]; ZPVE [kJ mol^{-1}]	G^{298} [a.u.]	$G^{298\ rel}$ [kJ mol^{-1}]
2c	-3542.52813	0	0; -; 1463	-3542.03505	0
TS2c	-3542.45773	185	1; -467; 1462	-3541.96282	190
15	-3542.50427	63	0; -; 1453	-3542.01670	48
14	-3760.11000	0	0; -; 1447	-3759.62408	0
TS3/14	-3760.08958	54	1; -202; 1442	-3759.60573	48
3	-3760.11906	-24	0; -; 1447	-3759.63259	-22
17M	-2450.01139	267	0; -; 403	-2449.89483	261
TS17M	-2449.97478	363	2; -135, -9.5; 402	-2449.85681	360
15M	-2450.07198	108	0; -; 407	-2449.95412	105
TS(2c/125)M	-2450.02981	218	1; -252; 401	-2449.91352	211
2cM	-2450.11300	0	0; -; 408	-2449.99405	0
TS3M	-2667.61467	188	2; -163, -1; 395	-2667.50070	191
3M	-2667.68380	7	0; -; 397	-2667.57074	7
TS(3/14)M	-2667.65056	94	1; -320; 393	-2667.53825	92
14M	-2667.68641	0	0; -; 397	-2667.57343	0

1,2 Borole shift in compound 2c (Boronotropic shift)

The high energy computed for the transition state TS**2c** ($\Delta E(TS\textbf{2c})$ = 185 kJ mol^{-1}, see Figure S22) of the borono-tropic shift along the η^1-bonded cyclopentadienyl substituent explains the non-equivalence of the cyclopentadiene carbon atoms in the $^{13}C\{^1H\}$ NMR spectra even at T = 70°C.
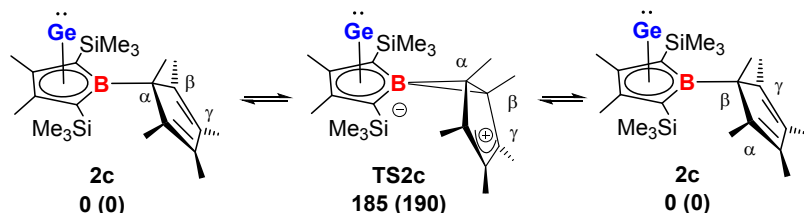

Figure S22. Boronotropic shift in compound **2c** (relative energies ΔE and relative free Gibbs enthalpies ΔG^{298} at T = 298K (in brackets, M06-2X/6-311+G(d,p)).
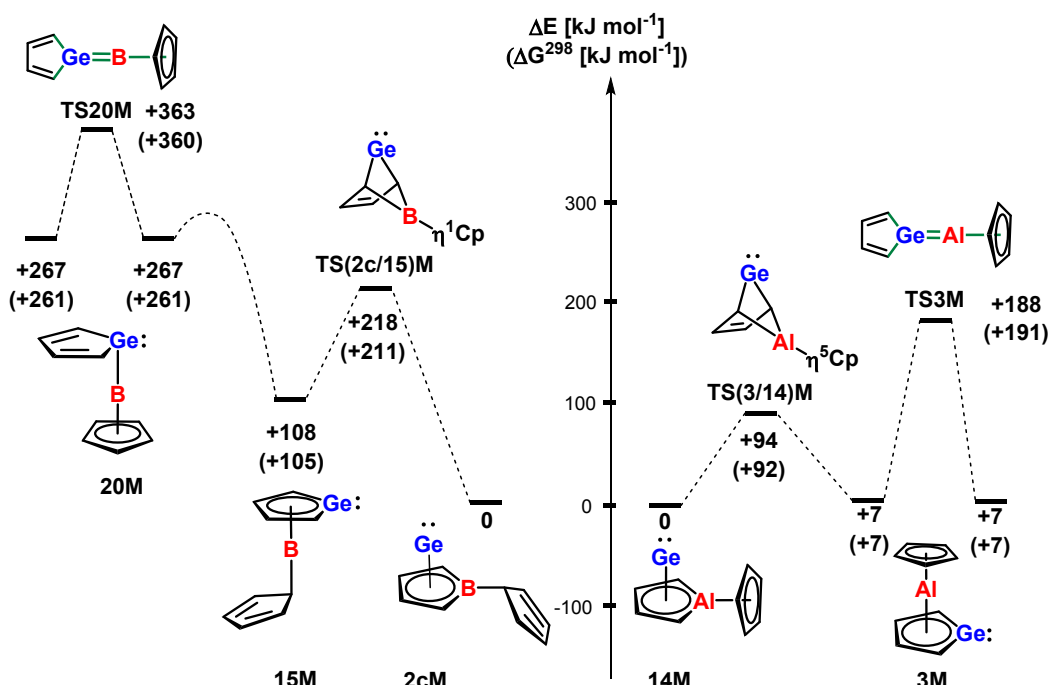

Figure S23. Reaction coordinates for the formation of the borole germanium(II) complex **2cM** and germaaluminocene **3M** (calculated at the M06-2X/6-311+G(d,p) level of theory) Y-shape arrangement in **TS20M** and **TS3M** is indicated by green bonds.

We studied the formation of germanium borole complex **2cM** and germaaluminocene **3M** computationally and the results are summarized in Figure S23. In contrast to classical boraalkenes **16**[27], borasilenes **17**[28], boragermenes **18**[29] and vinyl cations **19**[30], the related structures, **TS20M** and **TS3M** with an Y-shaped arrangement around the two heteroatoms, are not minima on the potential energy surfaces (PES). In the case of the boron compound, the linear structure is a high-lying transition state. The corresponding minimum structure **20M** with a η^1-coordinated germole ring and a η^5-bonded cyclopentadiene substituent shows clear similarities to borocenium cation **5** (Figure 2, main text). The hapticity change of the boron atom in **20M** between both cyclic ligands to give the η^5-germole complex **15M** is strongly exothermic (by 159 kJ mol^{-1}). The final germole to borole transformation via **TS(2c/15)M** is also highly exothermic and proceeds via a barrier of 110 kJ mol^{-1} (Figure S23). The corresponding PES of the aluminum compounds is shallower and involves a smaller number of species. The linear structure **TS3M** is the transition state for the degenerate face-shift of the CpAl group in germaaluminocene **3M**. Interestingly, the aluminocene **3M** is actually slightly less stable than the germanium alumole complex **14M** (by 7 kJ mol^{-1}) and the rearrangement **3M → 14M** is connected with a barrier of 87 kJ mol^{-1}. The reversal of the relative stability of the model compounds, germaaluminocene **3M** and germanium alumole complex **14M** compared to that of the experimentally investigated **3** and **14** suggests a decisive substituent effect on their relative stability.
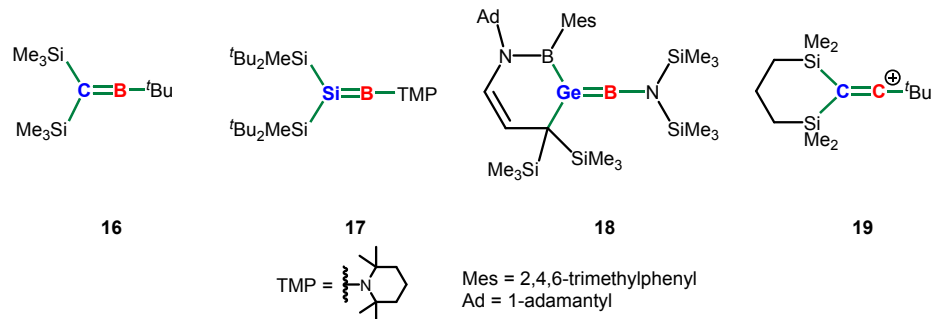

Figure S24. Compounds relevant fort the discussion (Y-shaped arrangement indicated by green bonds).

References.

1. Z. Dong, C. R. W. Reinhold, M. Schmidtmann and T. Müller, *Organometallics*, 2018, **37**, 4736-4743.
2. P. Jutzi, B. Krato, M. Hursthouse and A. Howes, *Chem. Ber.*, 1987, **120**, 565.
3. H.-J. Koch, S. Schulz, H. W. Roesky, M. Noltemeyer, H.-G. Schmidt, A. Heine, R. Herbst-Irmer, D. Stalke and G. M. Sheldrick, *Chem. Ber.*, 1992, **125**, 1107-1109.
4. G. M. Sheldrick, *Journal*, 2014.
5. G. Sheldrick, *Acta Crystallogr., Sect. C: Cryst. Struct. Commun.*, 2015, **71**, 3-8.
6. C. L. B. Macdonald, J. D. Gorden, A. Voigt, S. Filipponi and A. H. Cowley, *Dalton Trans.*, 2008, 1161-1176.
7. J. D. Gorden, A. Voigt, C. L. B. Macdonald, J. S. Silverman and A. H. Cowley, *J. Am. Chem. Soc.*, 2000, **122**, 950-951.
8. A. Haaland, K.-G. Martinsen, S. A. Shlykov, H. V. Volden, C. Dohmeier and H. Schnöckel, *Organometallics*, 1995, **14**, 3116-3119.
9. P. Tholen, Z. Dong, M. Schmidtmann, L. Albers and T. Müller, *Angew. Chem. Int. Ed.*, 2018, **57**, 13319-13324.
10. C. P. Sindlinger and P. N. Ruth, *Angew. Chem. Int. Ed.*, 2019, **58**, 15051-15056.
11. T. Agou, T. Wasano, P. Jin, S. Nagase and N. Tokitoh, *Angew. Chem. Int. Ed.*, 2013, **52**, 10031-10034.
12. a) C. Dohmeier, H. Schnöckel, U. Schneider, R. Ahlrichs and C. Robl, *Angew. Chem. Int. Ed.*, 1993, **32**, 1655-1657; b) R. W. Schurko, I. Hung, C. L. B. Macdonald and A. H. Cowley, *J. Am. Chem. Soc.*, 2002, **124**, 13204-13214.
13. J. D. Gorden, C. L. B. Macdonald and A. H. Cowley, *Chem. Commun.*, 2001, 75-76.
14. J. Gauss, U. Schneider, R. Ahlrichs, C. Dohmeier and H. Schnöckel, *J. Am. Chem. Soc.*, 1993, **115**, 2402-2408.
15. J. D. Fisher, P. H. M. Budzelaar, P. J. Shapiro, R. J. Staples, G. P. A. Yap and A. L. Rheingold, *Organometallics*, 1997, **16**, 871-879.
16. G. W. T. M. J. Frisch, H. B. Schlegel, G. E. Scuseria, M. A. Robb, J. R. Cheeseman, G. Scalmani, V. Barone, G. A. Petersson, H. Nakatsuji, X. Li, M. Caricato, A. V. Marenich, J. Bloino, B. G. Janesko, R. Gomperts, B. Mennucci, H. P. Hratchian, J. V. Ortiz, A. F. Izmaylov, J. L. Sonnenberg, D. Williams-Young, F. Ding, F. Lipparini, F. Egidi, J. Goings, B. Peng, A. Petrone, T. Henderson, D. Ranasinghe, V. G. Zakrzewski, J. Gao, N. Rega, G. Zheng, W. Liang, M. Hada, M. Ehara, K. Toyota, R. Fukuda, J. Hasegawa, M. Ishida, T. Nakajima, Y. Honda, O. Kitao, H. Nakai, T. Vreven, K. Throssell, J. A. Montgomery, Jr., J. E. Peralta, F. Ogliaro, M. J. Bearpark, J. J. Heyd, E. N. Brothers, K. N. Kudin, V. N. Staroverov, T. A. Keith, R. Kobayashi, J. Normand, K. Raghavachari, A. P. Rendell, J. C. Burant, S. S. Iyengar, J. Tomasi, M. Cossi, J. M. Millam, M. Klene, C. Adamo, R. Cammi, J. W. Ochterski, R. L. Martin, K. Morokuma, O. Farkas, J. B. Foresman, D. J. Fox, Gaussian, Inc., Wallingford CT, 2016, *Gaussian 16 Revision A.03*.
17. A. E. Reed, L. A. Curtiss and F. Weinhold, *Chem. Rev.*, 1988, **88**, 899-926.
18. G. W. T. M. J. Frisch, H. B. Schlegel, G. E. Scuseria, M. A. Robb, J. R. Cheeseman, G. Scalmani, V. Barone, B. Mennucci, G. A. Petersson, H. Nakatsuji, M. Caricato, X. Li, H. P. Hratchian, A. F. Izmaylov, J. Bloino, G. Zheng, J. L. Sonnenberg, M. Hada, M. Ehara, K. Toyota, R. Fukuda, J. Hasegawa, M. Ishida, T. Nakajima, Y. Honda, O. Kitao, H. Nakai, T. Vreven, J. A. Montgomery, Jr., J. E. Peralta, F. Ogliaro, M. Bearpark, J. J. Heyd, E. Brothers, K. N. Kudin, V. N. Staroverov, T. Keith, R. Kobayashi, J. Normand, K. Raghavachari, A. Rendell, J. C. Burant, S. S. Iyengar, J. Tomasi, M. Cossi, N. Rega, J. M. Millam, M. Klene, J. E. Knox, J. B. Cross, V. Bakken, C. Adamo, J. Jaramillo, R. Gomperts, R. E. Stratmann, O. Yazyev, A. J. Austin, R. Cammi, C. Pomelli, J. W. Ochterski, R. L. Martin, K. Morokuma, V. G. Zakrzewski, G. A. Voth, P. Salvador, J. J. Dannenberg, S. Dapprich, A. D. Daniels, O. Farkas, J. B. Foresman, J. V. Ortiz, J. Cioslowski, D. J. Fox, Gaussian, Inc., Wallingford CT, 2013., *Gaussian 09 Revision D.01*.
19. E. D. Glendening, J. K. Badenhoop, A. E. Reed, J. E. Carpenter, J. A. Bohmann, C. M. Morales, C. R. Landis and F. Weinhold, personal communication.

20. R. F. W. Bader, Atoms in Molecule: A Quantum Theory, Clarendon Press, Oxford, U.K., 1990.
21. Jmol, an open-source Java viewer for chemical structures in 3D. http://www.jmol.org.
22. Y. Zhao and D. Truhlar, *Theor. Chem. Acc.*, 2008, **120**, 215-241.
23. a) K. Fukui, *Acc. Chem. Res.*, 1981, **14**, 363-368; b) H. P. Hratchian and H. B. Schlegel, in *Theory and Applications of Computational Chemistry*, eds. C. E. Dykstra, G. Frenking, K. S. Kim and G. E. Scuseria, Elsevier, Amsterdam, 2005, vol. 1, ch. 10, pp. 195-249.
24. H. Sitzmann, M. F. Lappert, C. Dohmeier, C. Üffing and H. Schnöckel, *J. Organomet. Chem.*, 1998, **561**, 203-208.
25. S. Krieck, H. Görls and M. Westerhausen, *Organometallics*, 2008, **27**, 5052-5057.
26. H. Nöth, *Z. Naturforsch. B*, 1980, **35**, 119.
27. R. Boese, P. Paetzold, A. Tapper and R. Ziembinski, *Chem. Ber.*, 1989, **122**, 1057-1060.
28. N. Nakata and A. Sekiguchi, *J. Am. Chem. Soc.*, 2006, **128**, 422-423.
29. B. Rao and R. Kinjo, *Angew. Chem. Int. Ed.*, 2019, **59**, 3147-3150.
30. T. Müller, M. Juhasz and C. A. Reed, *Angew. Chem. Int. Ed.*, 2004, **43**, 1543-1546.